Development and analytical validation of a finite element model of fluid transport through osteochondral tissue

[1]Brady D. Hislop
[1]Chelsea M. Heveran
[1,2,3]Ronald K. June

[1]Department of Mechanical & Industrial Engineering, Montana State University
[2]Department of Microbiology & Cell Biology, Montana State University
[3]Department of Orthopaedics and Sports Medicine, University of Washington

Corresponding Author
Ronald K June II
Assistant Professor, Mechanical and Industrial Engineering
Montana State University
PO Box 173800
Bozeman, MT 59717-3800
rjune@me.montana.edu
406.994.5941 (tel)
406.994.6292 (fax)

Keywords: cartilage mechanics; osteoarthritis; computational modeling; fluid flow; finite element modeling

Word count (Introduction through Discussion):

Abstract

Fluid transport between cartilage and bone is critical to joint health. The objective of this study was to develop and analytically validate a finite element model of osteochondral tissue capable of modeling cartilage-bone fluid transport. A biphasic viscoelastic model using an ellipsoidal fiber distribution was created with three distinct layers of cartilage, superficial zone, middle zone, and deep zone along with a layer of bone. For stress-relaxation in unconfined compression, our results for compressive stress, radial stress, effective fluid pressure, and elastic recoil were compared with established biphasic analytical solutions. Our model also shows the development of fluid pressure gradients at the cartilage-bone interface during loading. This model is the first to capture fluid pressure gradients at the cartilage-bone interface for unconfined compression. These results provide additional evidence that fluid is transported between cartilage and bone during loading. Our study examines fluid transport between cartilage and bone from a new perspective using viscoelastic assumptions, in contrast with previous models that used poroelastic models. Further our model incorporates an ellipsoidal fiber distribution for collagen fibers while a previous model used a volume element model. Understanding the velocity and flux of fluid transport between cartilage and bone is key to elucidating the role of transport between cartilage and bone in joint health.

Introduction

Joint injuries frequently progress to debilitating osteoarthritis (OA), a leading cause of disability worldwide. For example, 40% of patients who experience a traumatic joint injury will develop PTOA within 10 years[28]. With aging or after traumatic injuries, our joints undergo significant biological and mechanical alterations that can eventually lead to OA. Cartilage and subchondral bone serve as the key structural components of our joints, with cartilage serving as the load-bearing tissue and subchondral bone providing structural support. Cartilage is a smooth avascular tissue that relies on its surrounding environment for nourishment. The current paradigm for joint fluid transport is that cartilage receives its nutrients through the synovial fluid and lymph nodes[20]. By contrast, bone receives its nutrients through the vasculature. Bone serves as the mechanical foundation of the joint through which cartilage can transfer loads. Bone also serves as a reservoir of nutrients and cytokines vital to the overall health of bone and possibly cartilage.

Fluid transport between bone and cartilage has the potential to influence the mechanical and biological environment of joint tissues. Imaging studies of the cartilage-bone interface show diffusion of solute between the subchondral bone and calcified cartilage[21,22]. A previous finite element model simulating a nanoindentation experiment and unconfined compression showed fluid transport between cartilage and bone[27]. Although these data support fluid transport from cartilage to bone during loading and bone to cartilage upon unloading, there are still persistent questions surrounding this phenomenon. Specifically, a gap exists in our understanding of the fluid pressure gradients and elastic recoil upon unloading that drive joint fluid transport, and the implications of such transport between cartilage and bone. Despite recent evidence[27] that transport from cartilage to bone occurs during loading and from bone to cartilage upon unloading, the velocity vectors, flux, and relevance of this transport to the mechanical and chemical environment of the joint remain unknown. Fluid transport between cartilage and bone could transport soluble signals (*i.e.* cytokines) to the cartilage and drive a significant role in maintaining cartilage health. A second gap is that many prior models of cartilage mechanics do not consider the collagen ultrastructure. We address this here using an ellipsoidal fiber distribution.

A computational model of fluid transport across the bone-cartilage interface would provide key insights into the role of fluid transport in joint health. The overall objective of this study is to develop a finite element model of osteochondral tissue capable of modeling cartilage-bone fluid transport. Through this model, we can begin to understand the fluid velocity vectors and flux between cartilage and bone while also investigating the fluid pressure gradients that drive this fluid transport. We hypothesize that fluid is transported between cartilage and bone during physiological loading/unloading and is driven by cartilage elastic recoil. Therefore, the three goals of this study are: (i) develop a finite element model of fluid transport in osteochondral tissue mimicking an unconfined compression experiment at physiologically relevant loads (ii) validate the finite element model against established analytical solutions; and (iii) quantify fluid pressure gradients at the cartilage-bone interface.

Materials and Methods

Model Geometry

Osteochondral cylinders (1mm diameter and 4mm height) were modeled in FEBio[18] using quarter symmetry (Figure 1). Boundary conditions simulated unconfined compression with impermeable boundaries and fixed displacements perpendicular to each side. To minimize nonlinear effects and computational complexity, a single body geometry was selected with hexahedral and penta mesh elements. Spatially dependent cartilage and bone material models were defined according to a 50-15-25-10 percentage split of bone, deep, middle, and superficial cartilage zones, respectively, (Figure 1) using an in-house MATLAB code.

Cartilage constitutive model and material properties

A viscoelastic neo-Hookean ellipsoidal fiber distribution model[3,4,20] was chosen for cartilage. Such modeling combines the tensile properties of collagen fibers and the viscoelastic response of the remaining matrix components and their bound water. The viscoelastic neo-Hookean model of the remaining matrix was applied to each layer of the tissue (v=0.499, relaxation time = 120s)[15]. A depth-dependent elastic modulus of the tissue was derived and applied to each layer of cartilage, using data from Walhquist *et al*.[26]:

$$E(MPa) = 5.839 - 5.7766Z + 4.0239Z^2 - 1.3551Z^3$$

where Z is the depth from the cartilage-bone interface. In addition, an ellipsoidal fiber distribution[3,4] was applied to each layer of cartilage independently with superficial zone fibers parallel to the superficial surface ($\beta = (2.5,2.5,2.5), \zeta = (4,4,2)$), middle zone fibers uniformly distributed ($\beta = (3.5,3.5,3.5), \zeta = (4,4,4)$), and deep zone fibers perpendicular to the superficial surface $\left(\beta = (2.5,2.5,2.5), \zeta = (2,2,4)\right)$, with β defining the elastic modulus along each axis and ζ defining the spatial distribution of fibers. The biphasic nature of the tissue was accounted for through the implementation of the Holmes-Mow permeability function[10], modeling the strain-dependent permeability of cartilage ($k_o = 6.2e^{-16}, M = 0.4, \alpha = 2.2$), with $k_o$defining the initial permeability, α defines the rate at which permeability approaches zero, and M is constant for the exponential fit.

Bone constitutive model and material properties

Previous computational studies of the osteochondral tissues have modeled bone as a rigid body given the large difference in modulus between cartilage and bone (bone ~1000x greater) between cartilage and bone. However, rigid body mechanics cannot be adapted for biphasic materials. Therefore, the bone was modeled as a biphasic isotropic elastic material (E= 17GPa, v= 0.29, φ= 5.5%)[1,27] throughout the geometry. Isotropic elastic models are considered effective for modeling the mechanical properties of bone[8,9] while allowing for the implementation of biphasic properties. Given the relatively low levels of bone deformation during the simulated loading, the bone permeability was spatially constant ($1e^{-17}$)[27].

Verification and model studies

Stress-relaxation was simulated using two simulation steps: a ramped compression step followed by a hold at 10% strain for 400s. Vertical and radial mesh convergence studies were performed to determine the appropriate mesh size for this model. Effective fluid pressures of each mesh were studied to determine the appropriate mesh size, using a threshold of <5% change to determine convergence. Additionally, a radial size study was performed to determine the effects of various radii on the physical parameters of the model. Each model's results were analyzed for vertical and radial stress relaxation, radial elastic recoil, effective fluid pressure relaxation, and differences in these physical parameters for the various radii to compare against validated analytical solutions[2]. Analytical predictions included Poisson's-ratio dependent elastic recoil and increasing radial elastic recoil with decreasing Poisson's ratio. Further analytical predictions included increased magnitude of compressive stress with increased radius. All results during this study were analyzed in PostView[14] a post-processing software developed to support FEBio. All simulations were run on the Hyalite Cluster at Montana State University[28] using 8 cores and 4GB RAM per core to achieve rapid solutions (~4 hrs).

Results

Mesh Convergence

Evaluation of the effective fluid pressure across three vertical mesh sizes (100, 200, 300) revealed a <5% increase in effective fluid pressure between 100 and 200 mesh stacks, and 200 and 300 mesh stacks (Sup. Figure 1B). Whereas, in the radial mesh study (8, 12, 16 radial slices) we saw increases in effective fluid pressure of 11.1% and 4.7% between 8 and 12, 12 and 16, respectively (Sup. Figure 1A). Given these results, we built our mesh with 8 theta segments, 12 radial slices, and 100 z-mesh stacks.

Compressive stress relaxation:

Compressive stress relaxation in the z-direction was observed within both cartilage and bone elements. Detailed inspection along the radial edge revealed z-direction relaxation throughout each layer of cartilage (superficial, middle, and deep; Figure 2A-F). While further evaluation revealed stress relaxation along the midline and center of the tissue for each layer (supplemental movie 1). Additionally, stress relaxation was observed throughout the bone, with decreasing levels of compressive stress with depth from the cartilage-bone interface.

Radial mesh studies revealed identical relaxation profiles across each radial mesh size (1, 0.75 and 0.5 mm). We also found that levels of compressive stress had a direct relationship with decreases in radial mesh size. Suggesting that our mesh size is appropriate for modeling the expected decreases in compressive stress with reductions in the radius of the model. Additionally, using a stretched exponential function[11] we found a relaxation time constant of 969.5 seconds.

Radial stress relaxation:

Radial stress relaxation at the radial edge (r=R) of cartilage was observed through each layer of the tissue. The middle zone of cartilage showed negative overall radial stress (Figure 3C-D), while the superficial zone showed an increase in radial stress from 0.5 mm to 1 mm (Figure 3F). Similar relaxation was seen at the radial edge of bone throughout most of the depth. However, near the bottom of the bone, a wave response was observed following the initial load.

Slight deviations in normalized relaxation profiles were observed between each radial mesh size with increases in relaxation time as the radius decreased in the deep zone of cartilage (Figure 3A). Similar to the effective pressure and compressive stress radial stress has a direct relationship with decreases in radial mesh size.

Effective Fluid pressure relaxation:

Effective fluid pressure relaxation was observed throughout cartilage and bone following the initial loading of cartilage. Analysis of the radial edge revealed fluid pressure relaxation for each layer of cartilage (Figure 4A-F) and radial mesh size. In addition, analysis of the midline and center of cartilage revealed similar patterns of fluid pressure relaxation. Likewise, analysis of bone at the radial edge and along the midline revealed fluid pressure relaxation throughout the bone. Additional analysis showed that pressure relaxation along the center of bone transitioned from negative to positive with depth from the cartilage-bone interface.

Fluid pressure relaxation profiles were found to be similar for each of the radial mesh sizes (1, 0.75, 0.5mm) studied, with R = 0.5 mm having the highest relative relaxation after 400s (Figure 4A). Additionally, consistent with the results seen for compressive stress the effective fluid pressure has a direct relationship with decreases in radial mesh size.

Elastic Recoil:

Elastic recoil of cartilage (v=0.499) at the radial edge was nonexistent (Figure 5A-C), whereas bone (v=0.29) (Figure 5D) underwent elastic recoil consistent with analytical solutions for biphasic materials[2]. We also found that levels of radial displacement decreased concurrently with a radial size consistent with the changes in compressive stress levels. Elastic recoil for cartilage was consistent across each of the radial mesh sizes and cartilage layers (Figure 5A-C). Conversely, bone recoil is the same across the 0.75- and 1-mm with changes in levels of recoil occurring only for the 0.5 mm model.

Fluid Pressure Gradients:

Cartilage fluid pressures at the cartilage-bone interface are consistently higher than bone immediately following the initial loading period (t=1 second) (Figure 6A). We also found

that fluid pressure gradients decreased after the 400 second relaxation period (t = 402.5 seconds) (Figure 6B).

Discussion

The purpose of this study was to investigate fluid pressure gradients and cartilage elastic recoil in fluid transport across the cartilage-bone interface during unconfined compression experiments. Model results were consistent with analytical results for biphasic materials[2], including axial and radial stress relaxation, elastic recoil, and effective fluid pressure relaxation. Results for the radial stresses in the superficial and middle zones of cartilage can be explained by the collagen fiber orientation in each region. Greater distribution of the collagen fibers parallel to the cartilage surface in the superficial zone leads to lower radial stresses (Figure 3D). By contrast, the random distribution of fibers in the middle zone and increased modulus (3.5 MPa v. 2.5 MPa) leads to lower stress magnitudes and overall negative radial stresses. This model also captures the Poisson ratio-dependent characteristics of elastic recoil for bone and cartilage. Further, the cartilage relaxation time of 969 seconds was within 20% of a previous experimental study[26].

Modeling results at the cartilage-bone interface demonstrate that unconfined compression results in higher fluid pressures in the cartilage than bone. These results suggest that a fluid pressure gradient develops from cartilage to bone during loading (Figure 6A). Our results agree with Stender *et al* in that fluid is transported between cartilage and bone and this transport is driven by the development of fluid pressure gradients at the cartilage-bone interface. Stender *et al* presented models of both unconfined compression and spherical indentation toward understanding permeability in cartilage-bone fluid transport. Our model is also in agreement with these previous results on the direction of the fluid transport during loading, although our model predicts much lower levels (~500 fold decreased flux) of transport from cartilage to bone. This discrepancy may result from methodological differences in collagen fiber modeling with our model using an ellipsoidal fiber distribution and the previous model using a pyramidal volume element model. Additionally, our use of a viscoelastic model versus the previous models use of a poroelastic model may also be important. These discrepancies cause the mechanics of each model to differ and thus the fluid flux.

Our results challenge the previous understanding that fluid transport predominantly occurs between cartilage and synovial fluid. Cytokines and nutrients transported from subchondral bone to cartilage could be critical to the health and viability of chondrocytes. A previous study showed that increased hydrostatic pressures within cartilage was directly linked to production of proline an amino acid essential to collagen formation[21]. This study combined with our results and those of Stender *et al* suggest that fluid transport from subchondral bone to cartilage and within cartilage is critical to the health and viability of chondrocytes. The transfer of nutrients and cytokines from subchondral bone could provide biochemical energy and other chemical signals to chondrocytes. Transfer of fluid from subchondral bone in healthy joints during physiological loading could support chondrocyte health and viability by supplementing nutrient transfer from synovial fluid. However, fluid transfer from subchondral bone to cartilage

following traumatic injuries could also lead to an increased level of inflammatory cytokines in cartilage tissue that are linked to degradation of cartilage.

Our results also point to the intriguing possibility that altered fluid transport could participate in degenerative joint changes following injury. Recent studies demonstrate that the cartilage pericellular and extracellular matrices undergo significant alterations within three days after injury[5,7]. These extracellular matrix stiffness reductions could lead to increased interstitial fluid pressures that cause chondrocytes to experience higher local stresses. A previous study showed that chondrocyte metabolism is altered by fluid induced shear-stresses[22]. Our study combined with a study of the response of chondrocytes to adverse loading suggest that fluid induced shear stress below 15-20 (dyn/cm^2) a threshold value is healthy for chondrocytes[29]. Thus, increased interstitial fluid pressure following traumatic injury could drive the altered metabolic profile and viability of chondrocytes.

Changes to subchondral bone tissue after injury could also affect fluid transport across the joint. Subchondral bone goes through a transient phase after joint injury of thinning and loss of bone mineral before becoming sclerotic[13,16]. If bone acts as an 'overflow reservoir' for fluid in cartilage, changes in bone geometry and density could impact how fluid is transported between the two tissues. Increased or decreased transport could each affect cartilage loading and nutrition. An alternate possibility is that changes to fluid transport between cartilage and bone could promote these cartilage material property changes either through both direct and indirect (e.g., via transport of cytokines and enzymes) mechanisms. The role of changing fluid pressure in cartilage at early timepoints after joint injury is not yet determined and necessitates additional investigation.

Our model advances the understanding of fluid transport between bone and cartilage in several key ways. Using an ellipsoidal fiber distribution, we improved the modeling of collagen fibers within the cartilage tissue. This improvement is critical to osteochondral fluid transport models as it provides a better structural representation of the mechanics in cartilage that are directly tied to this transport. Our model also improves the understanding of the fluid pressure gradients that develop at the cartilage-bone interface during physiological loading. The implications of fluid transport between cartilage and bone on the health of these tissues, as well as in degenerative joint diseases, are not yet understood. Several critical questions remain about how fluid transport between subchondral bone and cartilage affects chondrocyte health and viability, how transport between subchondral bone and cartilage following traumatic injury leads to increased inflammatory stimuli (*e.g.* TNFα) and how transport between subchondral bone and cartilage in healthy joints affect chondrocyte viability? These questions motivate new directions in investigating the role of fluid transport as a relevant factor in multi-tissue whole-joint health.

Acknowledgements

We thank Dr. David Pierce for key insight and critical discussion in developing the model. Funding support provided by NSF (CMMI 1554708) and NIH (R01AR073964).

Conflict of Interest

Dr. June owns stock in Beartooth Biotech which was not involved in this study.

Table 1

Material	Elastic Modulus E	Poisson's Ratio v	Porosity
Bone	17 GPa	0.290	5.5%
Superficial Zone Cartilage	$5.8539 - 5.7766Z + 4.0239Z^2 - 1.3551Z^3$ (MPa)	0.499	73.0%
Middle Zone Cartilage	$5.8539 - 5.7766Z + 4.0239Z^2 - 1.3551Z^3$ (MPa)	0.499	81.0%
Deep Zone Cartilage	$5.8539 - 5.7766Z + 4.0239Z^2 - 1.3551Z^3$ (MPa)	0.499	86.0%

Figure 1

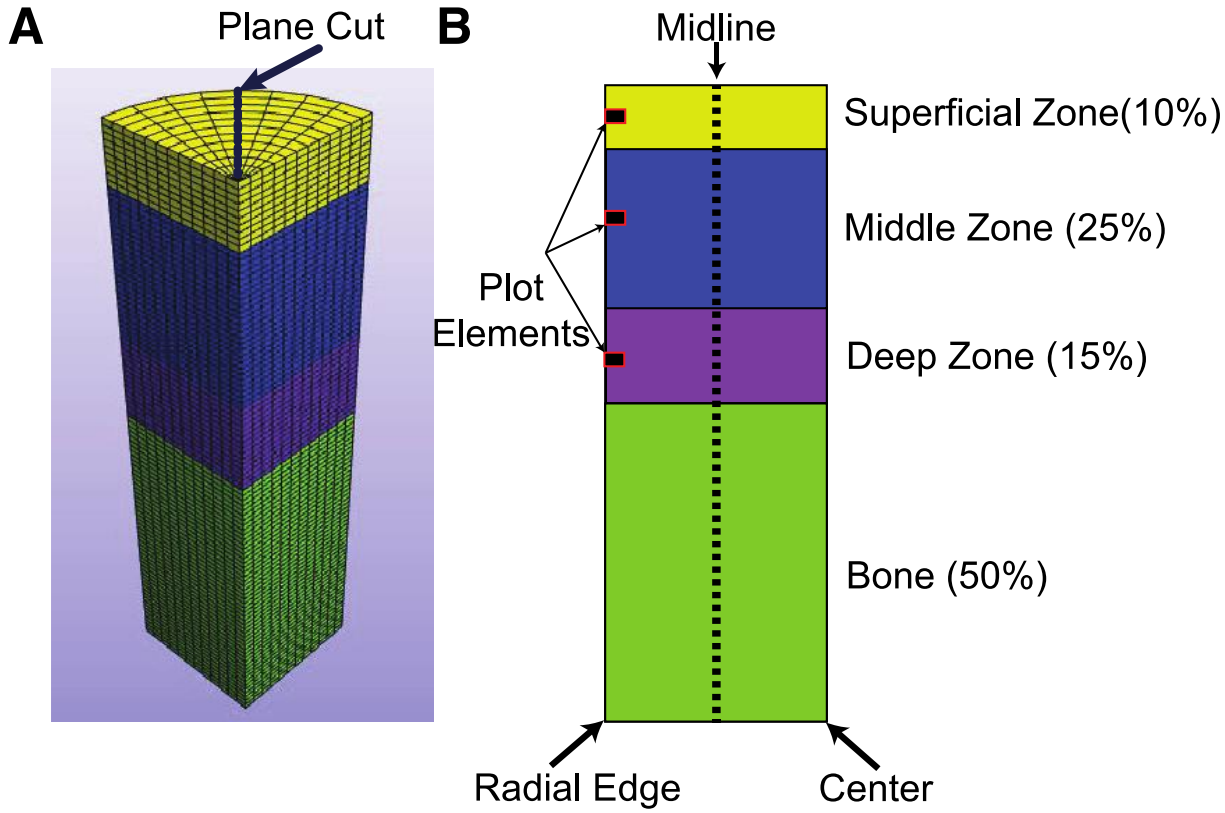

Figure 1 Finite element model of osteochondral tissue A) Mesh showing plane cut for evaluation; B) Schematic of cartilage layers and bone showing location of elements that are plotted in Figures 2-5.

Figure 2

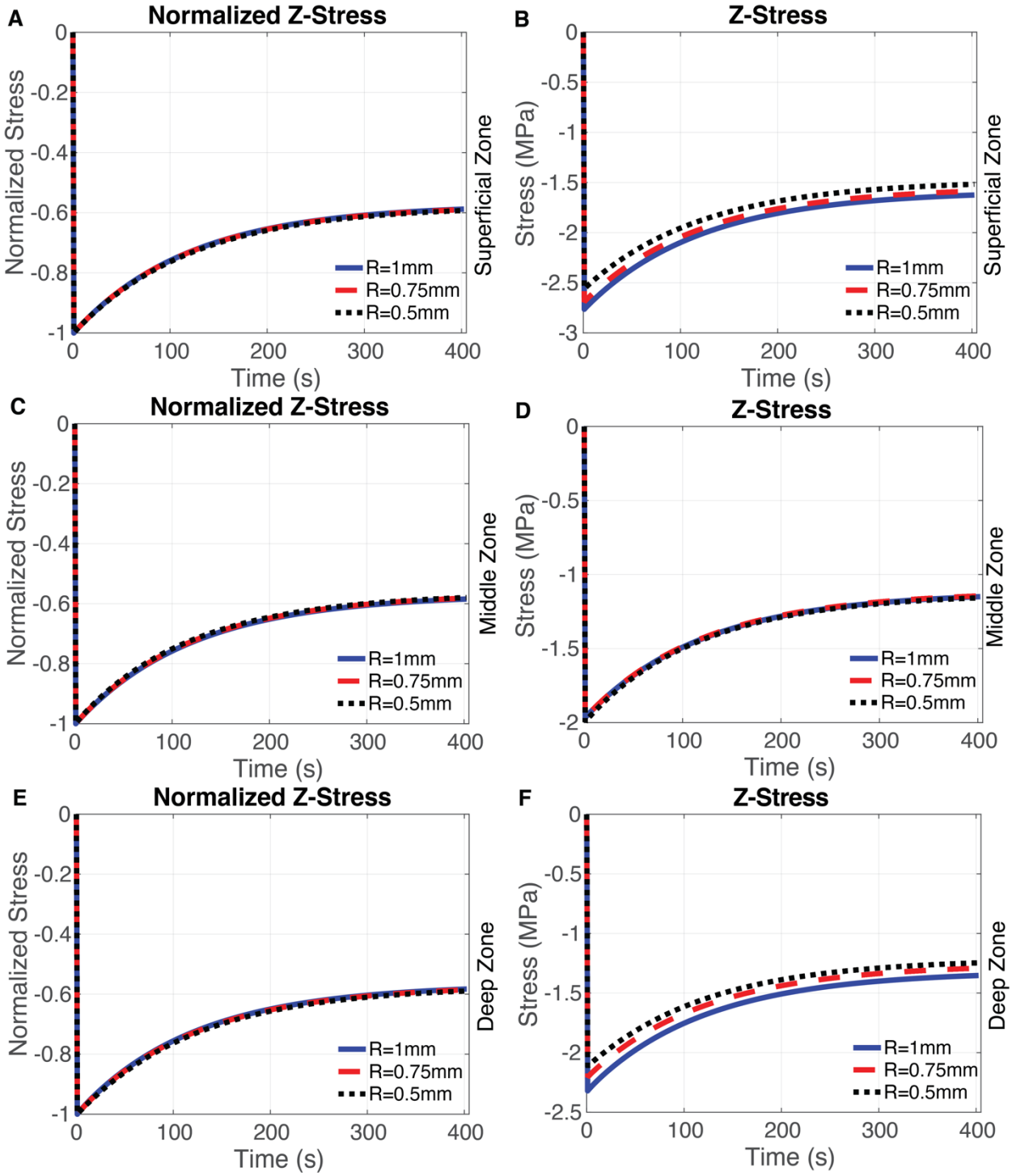

Figure 2 Compressive stress as a function of time for three radii. Normalized to peak compressive stress (left column) and absolute stress (right column) at location of interest and compressive stress at mid-depth of the superficial-zone (A-B), middle-zone (C-D), and deep-zone (E-F).

Figure 3

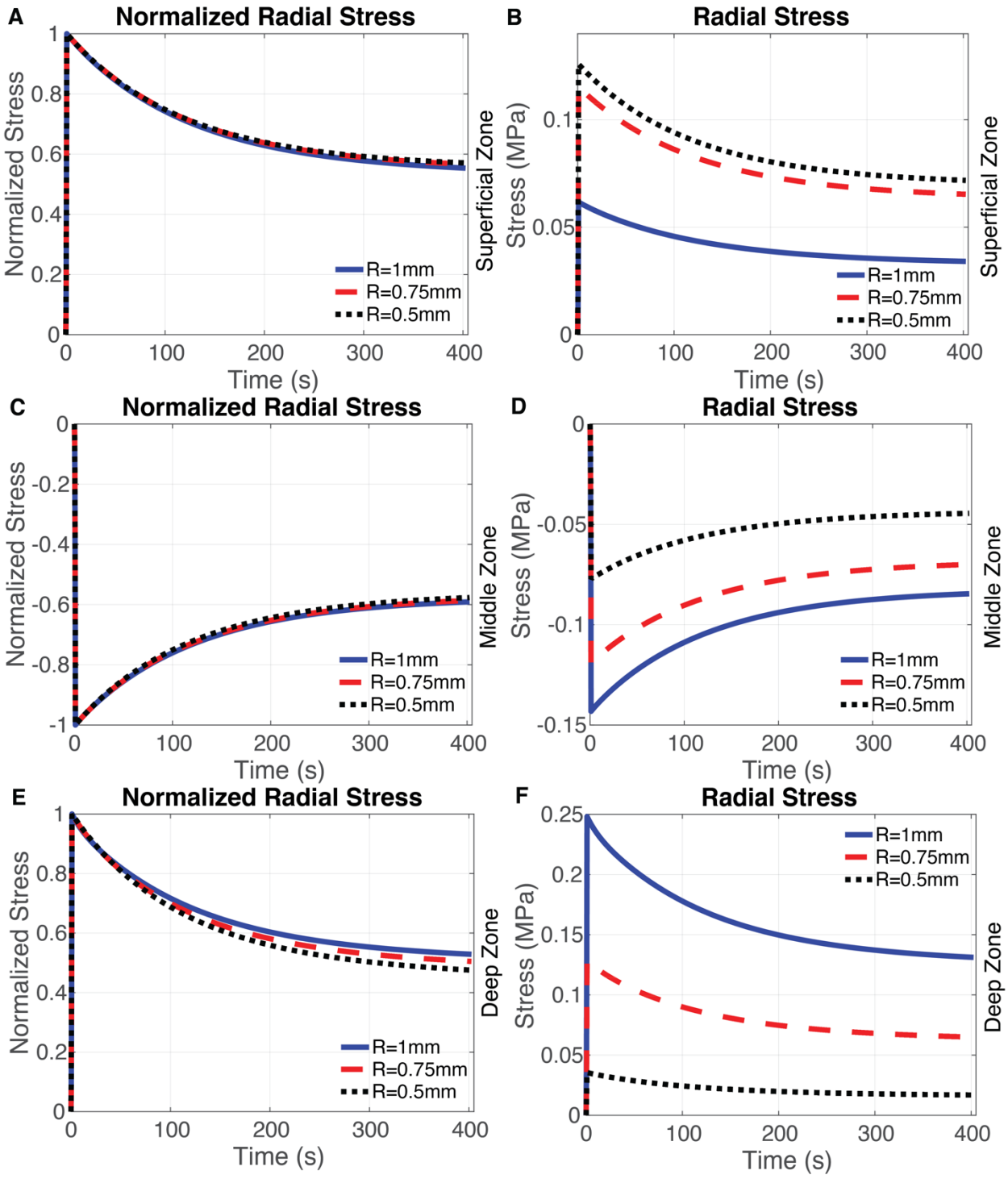

Figure 3 Radial stress as a function of time for three radii. Stress normalized to the peak radial stress at location of interest (left column) and absolute radial stress (right column) at the mid-depth of the superficial-zone(A-B), middle-zone (C-D), and deep-zone (E-F).

Figure 4

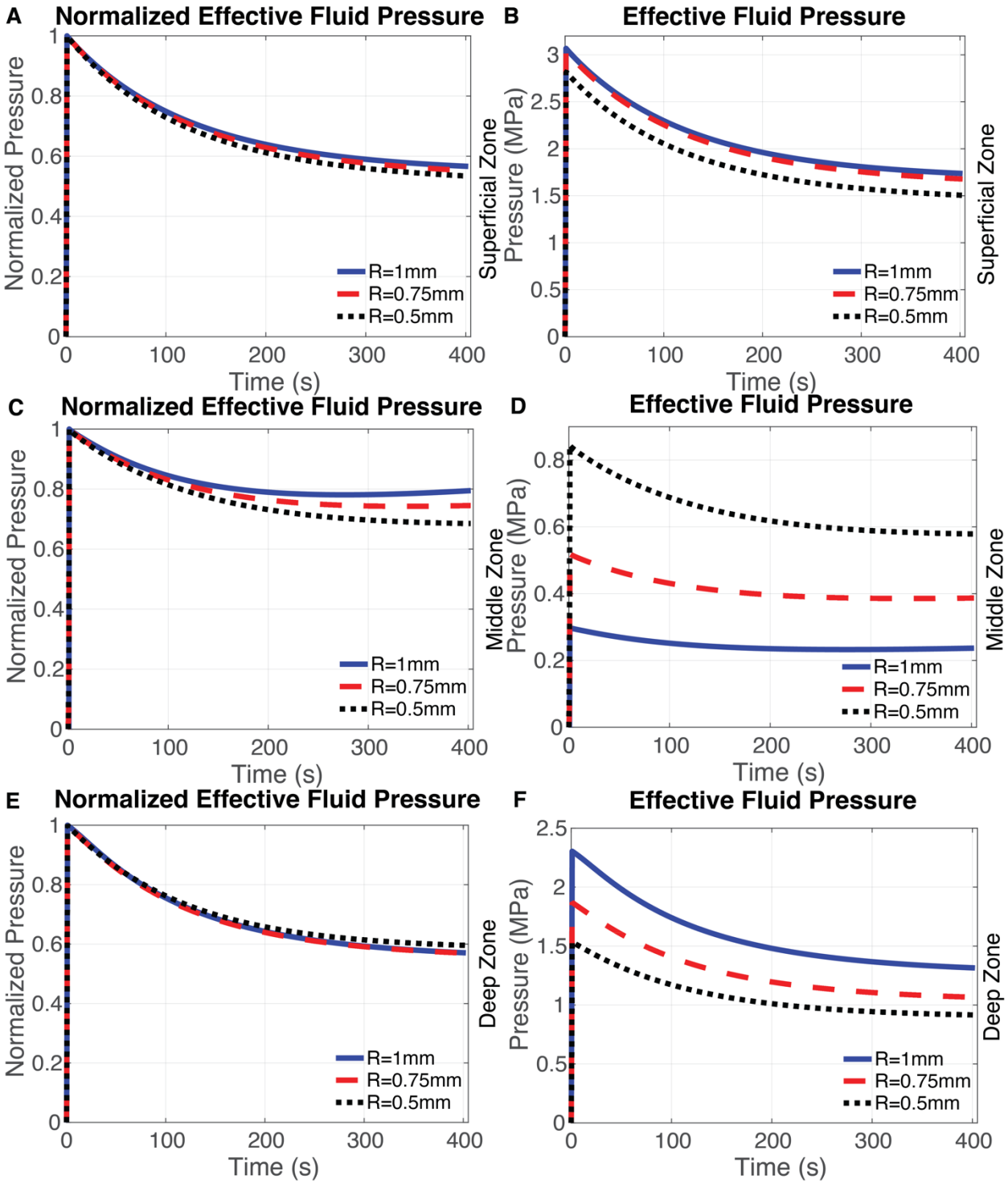

Figure 4 Effective Fluid pressure as a function of time for three radii. Fluid pressure normalized to peak effective fluid pressure (left column) and absolute effective fluid pressure (right column) at locations of interest at mid-depth of the superficial-zone (A-B), middle-zone (C-D), and deep-zone (E-F).

Figure 5

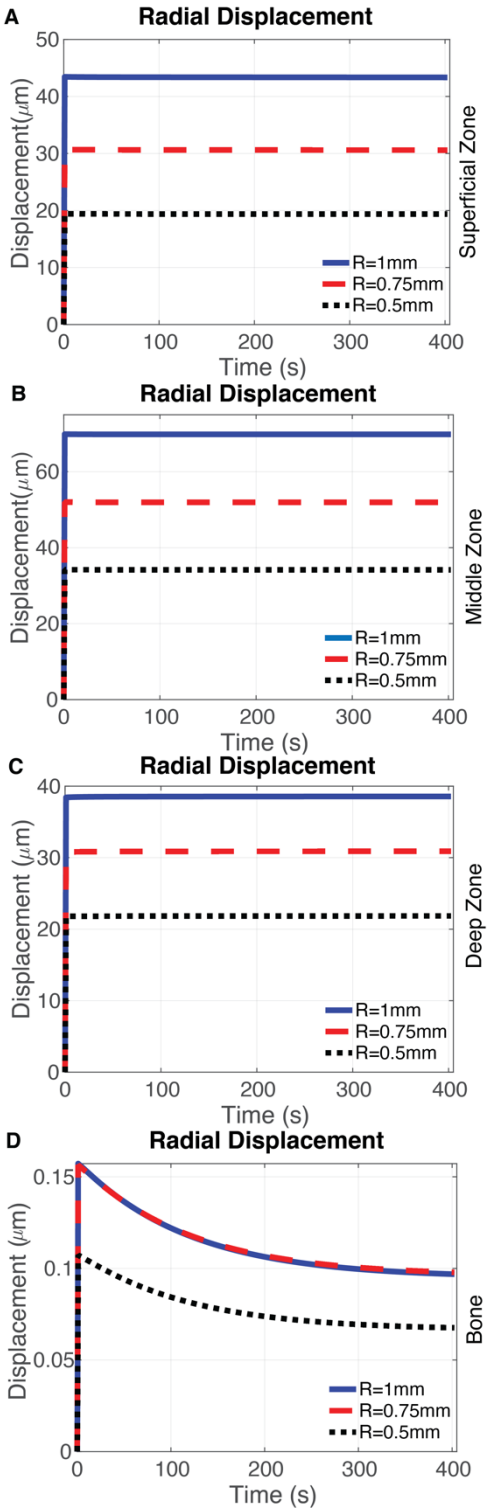

Figure 5 A-C: Radial Displacement of cartilage at mid-depth of superficial-zone, middle-zone and deep-zone for three radial mesh sizes; D: Radial Displacement of subchondral bone directly below cartilage for three radial mesh sizes.

Figure 6

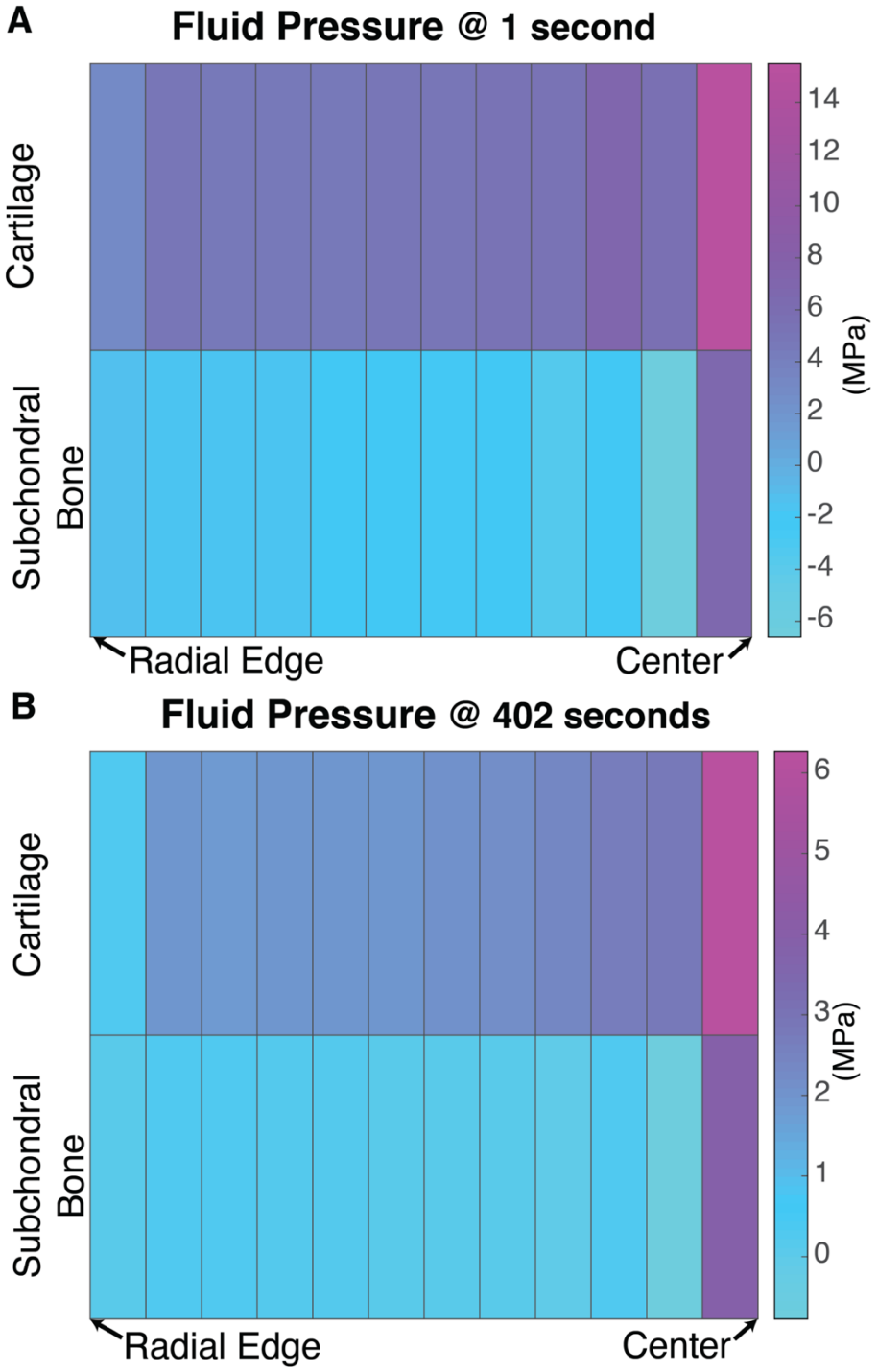

Figure 6 Mesh elements at the cartilage-bone interface A): Fluid pressures at cartilage-bone interface after initial load; B) Fluid pressure at cartilage-bone interface after 400 seconds of relaxation

Supplemental Figures

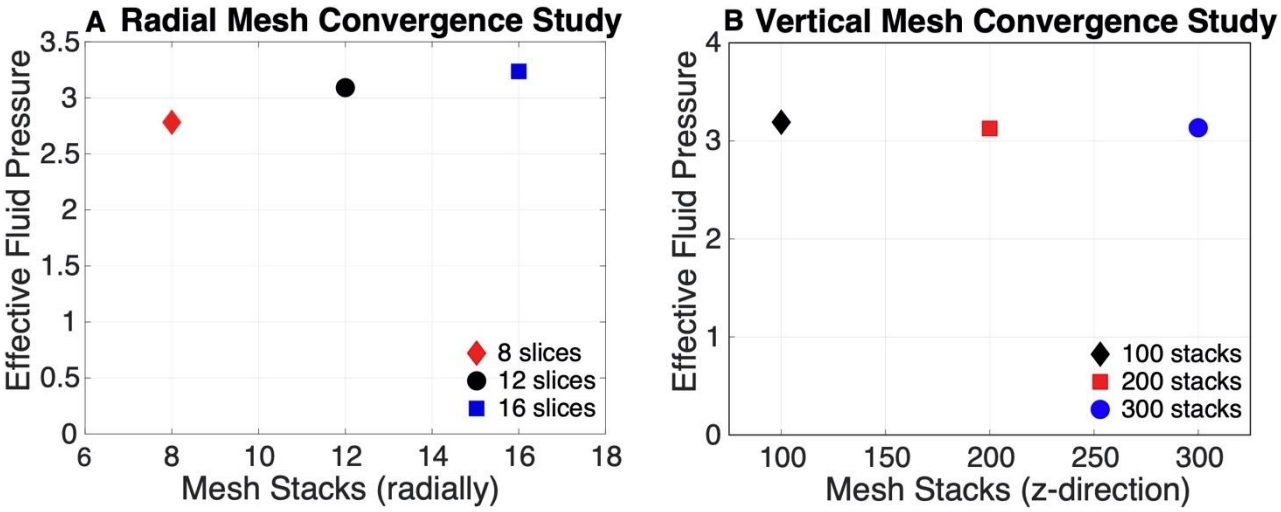

Supplemental Figure 1: A: Radial mesh convergence study of the effective fluid pressure; B: Vertical mesh convergence study of the effective fluid pressure.

References

[1]. Anderson, A. E., *et al*. (2008). "Validation of Finite Element Predictions of Cartilage Contact Pressure in the Human Hip Joint." Journal of Biomechanical Engineering 130(5): 10.

[2]. Armstrong, C. G., *et al*. (1984). "An Analysis of the Unconfined Compression of Articular Cartilage." Journal of Biomechanical Engineering 106: 165-173.

[3]. Ateshian, G. A. (2007). "Anisotropy of Fibrous Tissues in Relation to the Distribution of Tensed and Buckled Fibers." Journal of Biomechanical Engineering 129(2).

[4]. Ateshian, G. A., *et al*. (2009). "Modeling the Matrix of Articular Cartilage Using a Continuous Fiber Angular Distribution Predicts Many Observed Phenomena." Journal of Biomechanical Engineering 131(6).

[5]. Chery, D. R., *et al*. (2020). "Early changes in cartilage pericellular matrix micromechanobiology portend the onset of post-traumatic osteoarthritis." Acta Biomaterialia 111: 267-278.

[6]. Coleman, J. L., *et al*. (2013). "Diurnal variations in articular cartilage thickness and strain in the human knee." Journal of Biomechanics 46: 541-547.

[7]. Doyran, B., *et al*. (2017). "Nanoindentation modulus of murine cartilage: a sensitive indicator of the initiation and progression of post-traumatic osteoarthritis." Osteoarthritis and Cartilage 25: 10.

[8]. Harris, M. D., *et al*. (2012). "Finite Element Prediction of Cartilage Contact Stresses in Normal Human Hips." Journal of Orthopaedic Research

[9]. Henak, C. R., *et al*. (2014). "Finite Element Prediction of Transchondral Stress and Strain in the Human Hip." Journal of Biomechanical Engineering 136.

[10]. Holmes, M. H. and V. C. Mow (1990). "The nonlinear characteristics of soft gels and hydrated tissues in ultrafiltration." Journal of Biomechanics 23(11): 1145-1156.

[11]. June, R. K. and D. P. Fyhrie (2011). "A comparison of cartilage stress-relaxation models in unconfined compression: QLV and stretched exponential in combination with fluid flow." Computer Methods in Biomechanics and Biomedical Engineering 16(5): 565-576.

[12]. June, R. K., *et al*. (2009). "Cartilage stress-relaxation proceeds slower at higher compressive strains." Archives of Biochemistry and Biophysics 483: 6.

[13]. Lories, R. J. and F. P. Luyten (2011). "The bone-cartilage unit osteoarthritis." Nature Reviews 7: 43-49.

[14]. Maas, S. A., *et al*. (2017). "FEBio: History and Advances." Annual Review of Biomedical Engineering 19: 279-299.

[15]. Maas, S. A., *et al*. (2012). "FEBio: Finite Elements for Biomechanics." Journal of Biomechanical Engineering 134.

[16]. Mahjoub, M., *et al*. (2012). "Why Subchondral bone in osteoarthritis? The importance of the cartilage bone interface in osteoarthritis." Osteoporosis International 23: 842-846.

[17]. O'Hara, B. P., *et al*. (1990). "Influence of cyclic loading on the nutrition of articular cartilage." Annals of the Rheumatic Diseases 49.

[18]. Pan, J., *et al*. (2012). "Elevated cross-talk between subchondral bone and cartilage in osteoarthritic joints." Bone 212(7).

[19]. Pan, J., *et al*. (2009). "In situ measurement of transport between subchondral bone and articular cartilage." Journal of Orthopaedic Research: 1347-1352.

[20]. Pierce, D. M., *et al*. (2009). "A Phenomenological Approach Toward Patient Specific Computational Modeling of Articular Cartilage Including Collagen Fiber Tracking." Journal of Biomechanical Engineering 131.

[21]. Sah, R. L.-Y., *et al*. (1989). "Biosynthetic Response of Cartilage Explants to Dynamic Compression." Journal of Orthopaedic Research 7: 17.

[22]. Smith, R. L., *et al*. (1995). "Effects of Fluid-Induced Shear on Articular Chondrocyte Morphology and Metabolism In Vitro." Journal of Orthopaedic Research 13.

[23]. Soltz, M. A. and G. A. Ateshian (1998). "Experimental verification and theoretical prediction of cartilage interstitial fluid pressurization at an impermeable contact interface in confined compression." Journal of Biomechanics 31: 927-934.

[24]. Stender, M. E., *et al*. (2017). "A poroelastic finite element model of the bone-cartilage unit to determine the effects of changes in permeability with osteoarthritis." Computer Methods in Biomechanics and Biomedical Engineering 20(3): 319-331.

[25]. Thomas, A. C., *et al*. (2016). "Epidemiology of Posttraumatic Osteoarthritis." Journal of Athletic Training: 6.

[26]. Wahlquist, J. A., *et al*. (2017). "Indentation mapping revealed poroelastic, but not viscoelastic, properties spanning native zonal articular cartilage" Acta Biomaterialia, 64, 41-49

[27]. Wen, D., *et al*. (2009). "Lipids and Collagen Matrix Restrict the Hydraulic Permeability Within the Porous Compartment of Adult Cortical Bone." Annals of Biomedical Engineering 38(3): 558-569.

[28]. Hyalite Research Computing Cluster Montana State University. (https://www.montana.edu/uit/rci/hyalite/)

[29]. Healy., *et al.* (2005). “Divergent responses of chondrocytes and endothelial cells to shear stress: Cross-talk among COX-2, the phase 2 response, and apoptosis” Proceedings of the National Academy of Sciences. 102(39): 14010-14015